RESEARCH ARTICLE OPEN ACCESS

Enhancement of Electrochemical Performance of FeS_2 based Electrodes through Copper Doping

Sonali Das[1,§], Debayan Chatterjee[2,§,*]

1 (Advanced Technology Development Center (ATDC), Indian Institute of Technology (IIT), Kharagpur, India)
Email: sonalidas1303@gmail.com
2 (School of Nano Science and Technology (SNST), Indian Institute of Technology (IIT), Kharagpur, India)
Email: debayan.7.dc@gmail.com
** Corresponding author*
§ These authors contributed equally for the work

Abstract:
Since the electrode materials play the pivotal role in the electrochemical performance of supercapacitors, thus, FeS_2, a transition metal dichalcogenide (TMD), has been a cheap and simple candidate for the purpose owing to its abundance and facilitation of exhibiting redox reactions. The FeS_2 nanostructures were synthesized using a simple one-step solvothermal method and were observed to have ellipsoidal geometry. The problem of low conductivity of the FeS_2 based electrodes has been dealt with in the study by doping with copper which is a highly conducting metal. The Cu-doped FeS_2 exhibited a staggering near 50% increase in specific capacitance of 122 F g^{-1} over the undoped FeS_2 (61 F g^{-1}) maintaining the stability of the material for 200 cycles which paves a possible solution for electrode materials in pseudocapacitors.

Keywords **— pseudocapacitors, electrodes, doping, FeS_2**

I. INTRODUCTION

Supercapacitors have emerged as one of the most talked about devices in the recent years owing to their simplistic function and game-changing applications in an industrial context [1]. Supercapacitors (SCs) are electrochemical energy storage devices that store a high amount of energy and can deliver it at a rapid rate [5-6]. Typical energy storage devices such as conventional electric capacitors have energy densities ranging about 0.01 - 0.1 W h kg^{-1} while Li-ion batteries (LIBs) although have energy densities of 100 – 265 W h kg^{-1}, suffer tremendously in terms of power density and cycling stability [7,10]. A SC can store energy with density 1 – 10 W h kg^{-1} in gravimetric terms and deliver it ten times faster than a LIB [5]. SCs work on the principle of surface adsorption and formation of an electric double layer at the electrode-electrolyte interface thus, not involving any intercalation and deintercalation of ions into the bulk of the material thus, not exerting any stress on the material lattice in the bulk [5]. This is the reason SCs outperform batteries as far as cycling stability is concerned [7].

As we understand, it is the electrode material which plays the most eminent role in determining the performance of a SC. Generally, these devices are classified based on their electrode materials which significantly dictate their energy storing mechanism. There are crudely three types – Electric Double Layer Capacitors (EDLCs) [11] which store energy electrostatically within the nanoscale double layer without any chemical reactions, Pseudocapacitors [12-13], which store energy by means of charge transfer via Faradaic reactions occurring at the electrode-electrolyte interface, and hybrid supercapacitors [14], which work on a culmination of both principles stated above. Over the years, various materials have been tested in order to achieve the optimal electrochemical performance for high energy SCs. It has been observed that Faradaic materials such as metal oxides and chalcogenides have exhibited higher specific capacitance compared to EDLC-type materials such as carbon nanostructures [13].

TMDs are one of the candidates for electrode material owing to the multiple low-energy separated oxidation states of these metals which facilitates the redox reactions to take place. Sulphides, selenides and tellurides of various metals such as Fe, Ni, Co, Cu and Sn have been researched upon [27-29]. Iron being one of the cheapest and most easily available transition metals, fits in as a suitable option. The main problem with FeS_2 is its poor ionic conductivity and chances for material degradation [25]. Many complicated techniques have been investigated including but not limited to functionalization, making composites, morphological optimization and many more [31-37]. This paper encompasses the feasibility of using FeS_2 and enhancement of its electrochemical performance by means of doping with copper. Being a good conductor of electricity, Cu atoms can fill in some lattice sites to facilitate ionic charge transfer at the electrode interface thus, improving the ionic conductivity of the material. This would lead to an increase in the specific capacitance of the electrodes while maintaining its stability. In this work, a simple one-step solvothermal method has been

employed and the electrochemical performance of Cu-doped FeS_2 is compared to that of pristine FeS_2 which revealed a near 50% increase in the specific capacitance without any significant drop in the coulombic efficiency.

II. Materials and Methods

A. Materials

Iron Sulphate Heptahydrate ($FeSO_4.7H_2O$), Anhydrous Copper (II) Suphate ($CuSO_4$) and Sodium Thiosulphate Pentahydrate ($Na_2S_2O_3.5H_2O$) (99.99%, extrapure) were purchased from Merck. Ethylene Glycol (99.5%) was purchased from Sigma Aldrich.

B. Synthesis of pristine and Cu-doped FeS_2

Cu-doped FeS_2 nanostructures were prepared using solvothermal method similar to Wang et Al. [27]. First 20 mL ethylene glycol was added in 5 mL ethanol to form a solvent and set to magnetic stirring at room temperature. 1.25 g of $FeSO_4.7H_2O$, 1.24 g of $Na_2S_2O_3.5H_2O$ and 0.143 g of $CuSO_4$ was added to the prepared solvent and the solution was left stirring for 1 hour. The prepared solution was then transferred into a 40 mL Teflon lined stainless steel autoclave, then the solvothermal synthesis was carried out at 200 °C for 24 h in an oven. After naturally cooling to room temperature, the autoclave was opened. The precipitate was centrifuged and washed with distilled water and absolute ethanol three times each, respectively. Finally, the sample was collected and dried in vacuum at 80 °C for 6 h.

Pristine FeS_2 was also prepared using the same method only without the addition of $CuSO_4$.

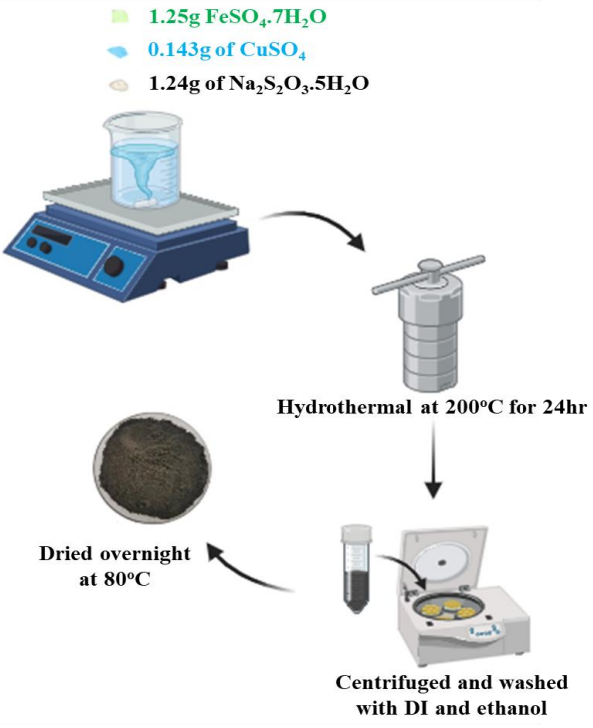

Figure 1: Schematic illustration of the synthesis route.

C. Physiochemical Characterization

The crystallographic information of the synthesized materials was extracted by X-ray diffraction (XRD) using a Rigaku Miniflex diffractometer with Cu-K_α (1.5406 Å) X-ray source. Fourier Transform Infrared (FTIR) spectroscopy was performed using a Shimadzu IR Spirit. The morphology of the synthesized structures was investigated by scanning electron microscopy using a SEM Carl Zeiss Supra 40. The N_2 adsorption-desorption isotherms were produced using Brunaer-Emmett-Teller (BET) technique at 77 K by a Quantachrome NOVA-Touch surface area and pore size analyser. X-ray photoelectron spectroscopy (XPS) data was generated using a PHI 5000 Versa Probe III system.

D. Electrochemical Characterization

Electrochemical measurements were performed in a three-electrode configuration, having Ag/AgCl in 3 M KCl as the reference electrode and platinum wire as the counter electrode. Working electrode was fabricated by preparing the slurry dissolving 80 wt% of active material (FeS_2), 10 wt% of polyvinylidene fluoride (PVDF) (binder) and 10 wt% activated carbon in acetone and continuously stirring for 2 h at 80 °C for complete homogeneity. The slurry was dropcasted on a 1 cm^2 graphite sheet and dried well at 80 °C. 1 M Na_2SO_4 was utilized as the electrolyte. The electrochemical estimations like cyclic voltammetry and galvanostatic charge-release estimates were performed using a Metrohm Autolab (PGSTAT302N).

III. Results and Discussions

A. Physiochemical Properties

The crystallographic features and phase purity of as-synthesized pristine and 10 % Cu-doped FeS_2 were assessed through XRD analysis. The obtained XRD patterns, depicted in Figure 2(a), were indexed using the JCPDS card no. 65-3321, corresponding to the isotropic cubic phase of FeS_2. In both samples, distinct peaks were observed around $2\theta = 29$, 33, 37, 47 and 56°, corresponding to (111), (200), (210), (220) and (311) planes, respectively. These could be attributed to the cubic phase of FeS_2. The addition of Cu introduced no additional peaks other than those present in pristine FeS_2 indicating that parent crystal structure remained unaltered even after doping since the ionic radii of the dopant ion is comparable to the host ion. There was no significant peak shift after doping. Furthermore, broadening of characteristic peaks in the doped sample suggested reduced crystallite size, particularly evident in case of the (210) and the (311) peaks.

Table 1: Crystallite Size and Lattice Parameter Specifications for Undoped and (10%) Cu-doped FeS_2.

Sample	Lattice Parameter (Å)	Crystallite size D (nm)
Pristine FeS_2	5.43	28.54
10% Cu-doped FeS_2	5.63	24.21

To determine the crystallite sizes, Scherrer's formula was applied using the most intense (200) peak for both samples. Results indicated a reduction in crystallite size from 28.54 nm for pristine FeS_2 to 24.20 nm for Cu-doped FeS_2, indicative of the influence of doping on crystalline domain size.

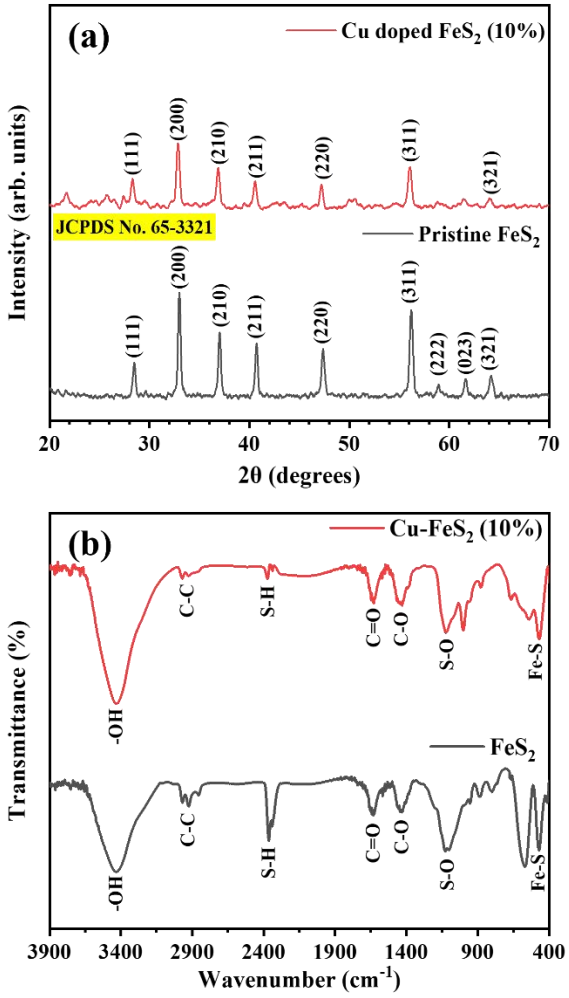

Figure 2: (a) XRD profiles and (b) FTIR spectra for pristine and 10% Cu-doped FeS_2.

From Figure 2(b), it can be seen that the most prominent peak indicates the Fe-S bond beyond 900 cm^{-1}. There are other peaks at 3400 cm^{-1} that indicate the presence of impurities such as moisture in the sample owing to its solvothermal synthesis protocol.

BET surface area experiments were performed by adsorption-desorption of N_2. The N_2 adsorption-desorption isotherms for all samples were recorded at 77 K and are shown in Figure 3. The estimated value of the specific surface area is 21.43 $m^2\ g^{-1}$ and 9.02 $m^2\ g^{-1}$ for doped and undoped samples, respectively. The average pore radii for both samples were observed to be approximately 1.58 nm. Hence, the microporous nature was confirmed.

Figure 4(a) shows a SEM micrograph of the 10% copper doped sample of FeS_2. The image clearly shows that nanoparticles with spherical and ellipsoidal shaped morphologies were formed which was in correspondence to the expected results. Also, the EDS spectrum of the same has been reported in Figure 4(b-d). The composition of elements is given in Table 2. The EDS spectrum shows a uniform distribution of both Fe and S. The presence of Cu was confirmed through EDS analysis of Cu-doped FeS_2.

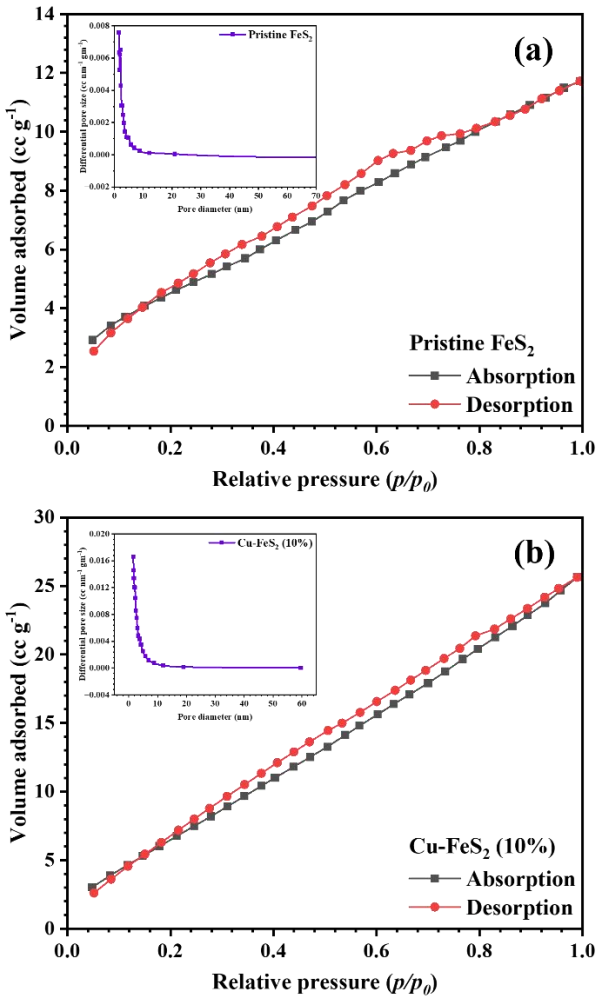

Figure 3: N_2 adsorption-desorption isotherms for (a) pristine FeS_2 and (b) 10% Cu-doped FeS_2 with their respective pore size distributions given in the insets.

XPS analysis was performed on the Cu-doped FeS_2 sample whose results are shown in Figure 5(a-d). XPS was operated at 15 kV with carbon 1s signal as the reference peak at a binding energy of 285 eV. Figure 5(a) shows the XPS survey spectrum which confirms the presence of Fe, S and Cu. The carbon peak was observed due to involvement of organic compounds during synthesis. The O 1s peak is observed due to exposure to moisture as synthesis was carried out in ambient atmosphere. Fe 2p peaks were observed at energies ~ 713 eV (Fe $2p_{3/2}$) and 723 eV (Fe $2p_{1/2}$) along with satellite peaks. Similarly, S_2^{2-} (disulphide) peaks were found at energies ~ 161 eV (S $2p_{3/2}$) and 162 eV (S $2p_{1/2}$). The confirmation of Cu replacing the Fe atom and formation of Cu

– S bond was revealed by Cu^{+} peaks at ~ 930 eV which indicated successful doping of Cu in FeS_2.

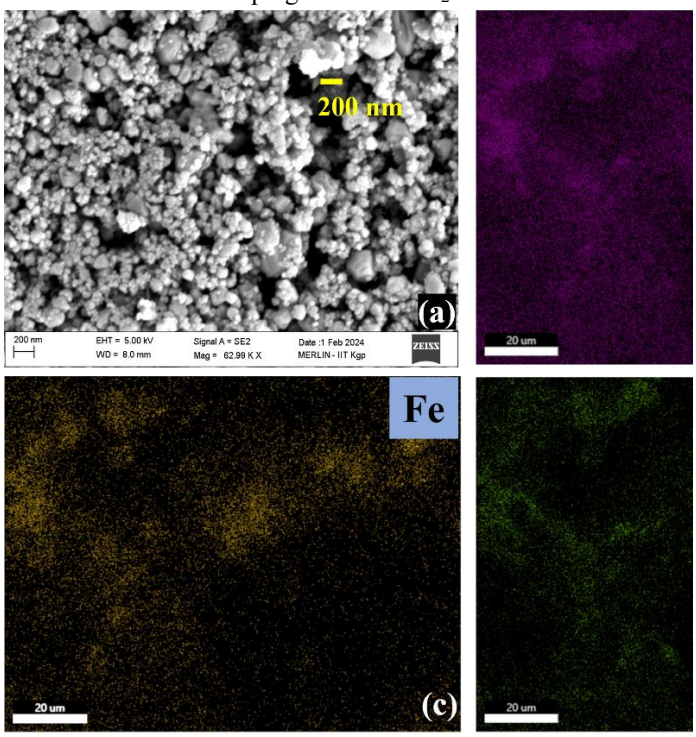

Figure 4: (a) SEM image of the 10% Cu-doped FeS_2 nanoparticles. (b-d) Elemental mapping by EDS for the elements S, Fe and Cu respectively.

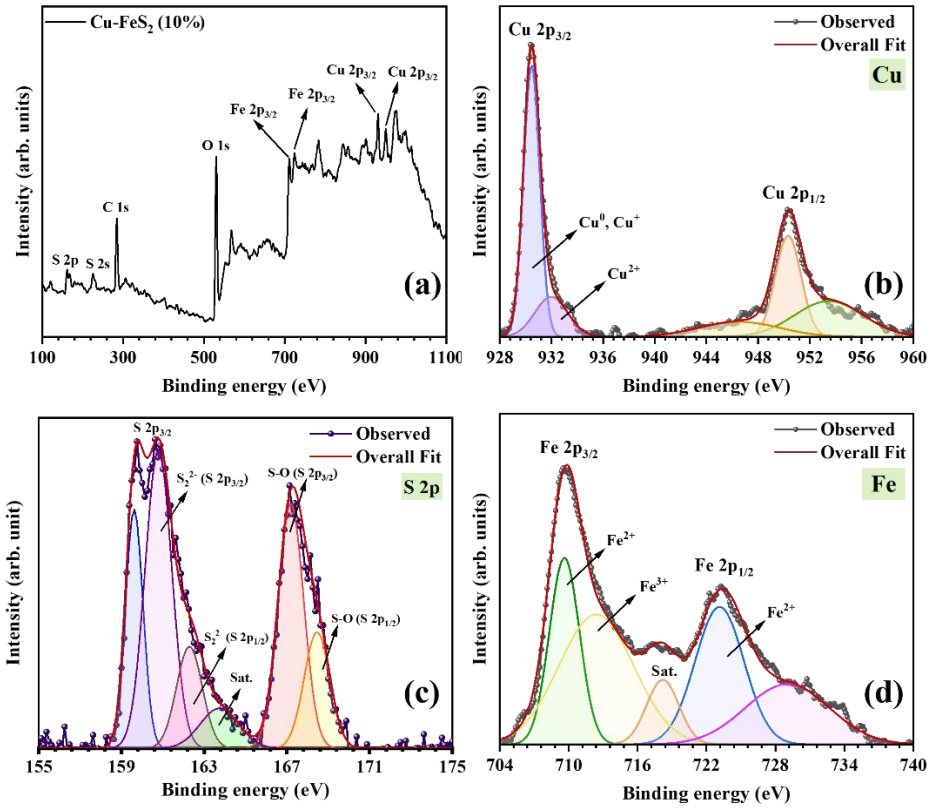

Figure 5: (a) XPS survey spectrum for 10% Cu-doped FeS_2. XPS spectra displaying peaks of (b) Cu 2p, (c) S 2p and (d) Fe 2p.

Table 2: Elemental Composition Determined from EDS Survey Scan Displaying Percentage of each Element Present.

Element	Composition (in %) as per EDS survey
Fe	65
S	24
Cu	11

B. Electrochemical Performance

The electrochemical analysis of both doped and undoped sample-based electrodes was performed in 1 M Na_2SO_4 electrolyte within an optimum potential window of 1.3 V. Figure 6 (a) & (b) show the cyclic voltammograms for scan rates varying from 5 to 200 mV s^{-1} for the pristine and Cu doped FeS_2 coated electrodes respectively. The cyclic voltammetry (CV) plots reveal a nearly rectangular curve, indicating the formation of a double-layer along with a slight deviation attributed to the pseudocapacitive component of energy storage. The specific capacitances for both samples were determined by calculating the area under the CV curves. For the doped sample, the maximum specific capacitance was measured to be 85 F g^{-1} at a scan rate of 5 mV s^{-1} and the same for the undoped sample was found to be 58 F g^{-1}. These findings demonstrate a higher capacity of Cu-doped sample compared to the pristine one. The results of the galvanostatic charge-discharge (GCD) are displayed in Figure 6 (c) and (d) for pristine and Cu-doped FeS_2 samples respectively. The maximum specific capacitance for the undoped and doped samples are 61 F g^{-1} and 122 F g^{-1} at 1 A g^{-1} current density respectively. The detailed results of GCD are given in Table 3. Further, Figure 7(a) and (b) clearly indicate that the 10% Cu-doped FeS_2 sample exhibits higher specific capacitances at all scan rates and all current densities compared to pristine FeS_2.

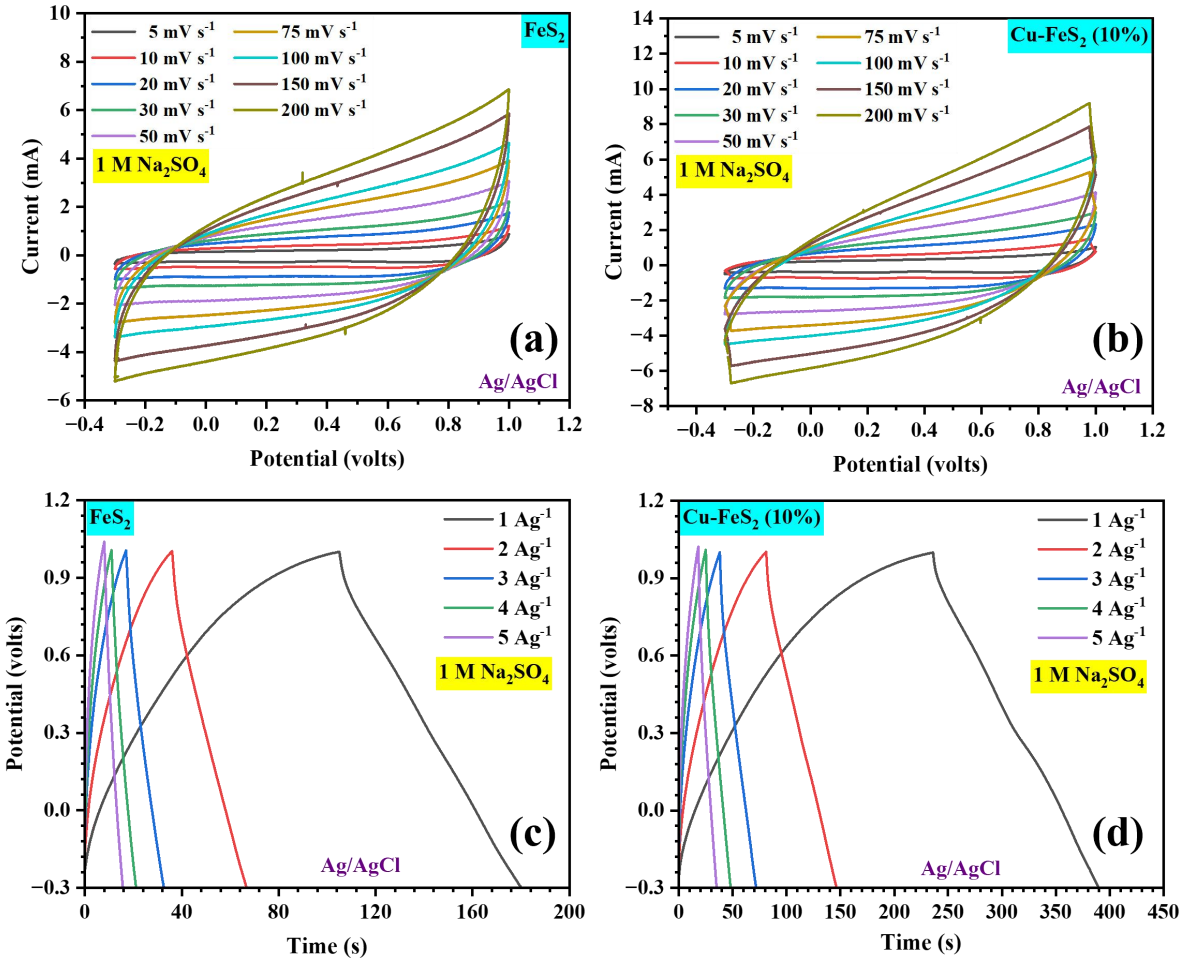

Figure 6: Cyclic voltammograms of (a) pristine and (b) 10% Cu-doped FeS_2 samples at different Scan Rates and Charge-Discharge profiles for (c) pristine and (d) 10% Cu-doped FeS_2 at different Current Densities in 1 M Na_2SO_4.

Table 3: Achieved Specific Capacitances for Pristine and 10% Cu-doped FeS_2 Samples at Different Current Densities.

Current Density (A g^{-1})	Specific Capacitance (F g^{-1}) Pristine FeS_2	Specific Capacitance (F g^{-1}) 10% Cu-doped FeS_2
1	61	122
2	52	108
3	43	86
4	42	84
5	40	77

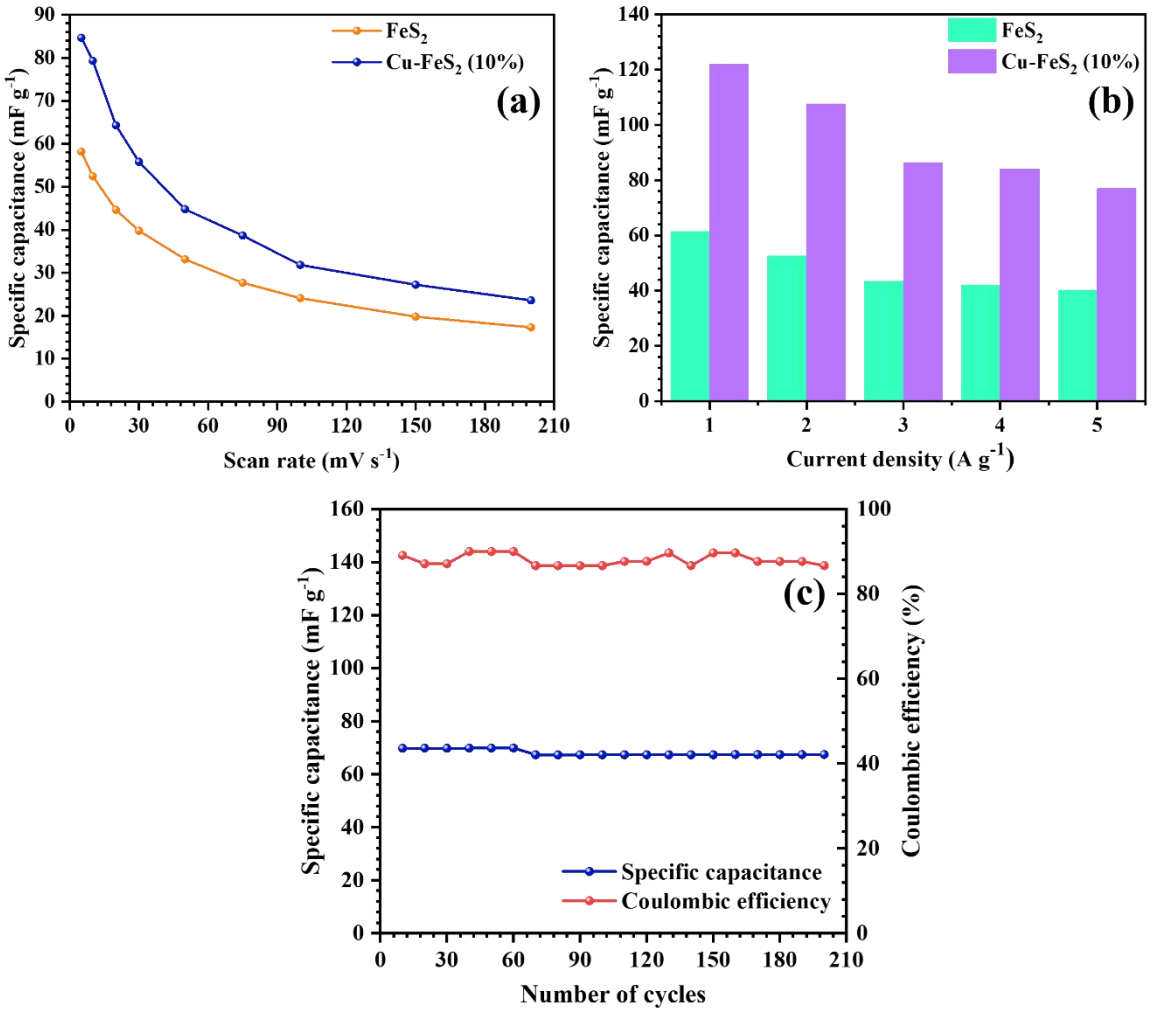

Figure 7: Comparative study of (a) Specific capacitance vs scan rates (b) Specific capacitance vs current density and (c) Cycling stability performance of the pristine and 10% Cu-doped FeS_2 at 3 A g^{-1} current density.

IV. Conclusion

This work establishes a novel strategy to synthesize the pristine and Cu-doped FeS_2 (10%) using a solvothermal method. XRD analysis of both the samples was carried out to confirm their phase. Further physiochemical characterizations of both the samples were performed such as FTIR, BET, XPS, SEM and EDS. Electrochemical characterization demonstrated a substantial enhancement in specific capacitance upon doping with copper, with a maximum

specific capacitance of 122 F g^{-1} for the 10% doped sample and of 61 F g^{-1} for the undoped sample at a current density of 1 A g^{-1} in 1 M Na_2SO_4. This nearly doubled capacity signifies the substantial enhancement of copper doping on the capacitive behaviour of FeS_2 electrodes. Moreover, cycling stability of the Cu-doped FeS_2 electrode revealed an 87% coulombic efficiency retention after 200 charge-discharge cycles, highlighting the durability and long-term stability of the electrode material.

Conclusively, the successful synthesis and comprehensive characterization of 10% Cu-doped FeS_2 electrodes have provided insights into the significant enhancement of electrochemical performance achieved through copper doping. These findings pave the way for further advancement in doping in FeS_2 based electrodes for supercapacitor.

ACKNOWLEDGEMENT

We put forward our sincere gratitude to the MEML Lab, Department of Physics, IIT Kharagpur and the Central Research Facility (CRF), IIT Kharagpur for providing us with all their experimental facilities and valuable guidance. But for their kindest support, this work would not have completed successfully.

REFERENCES

1. G. Wang, L. Zhang, and J. Zhang, "A review of electrode materials for electrochemical supercapacitors," *Chemical Society Reviews*, vol. 41, no. 2, pp. 797–828, 2012.
2. K. B. Oldham, "A Gouy–Chapman–Stern model of the double layer at a (metal)/(ionic liquid) interface," *Journal of Electroanalytical Chemistry*, vol. 613, no. 2, pp. 131-138, 15 February 2008.
3. Poonam, K. Sharma, A. Arora and S. Tripathi, "Review of supercapacitors: Materials and devices," *Journal of Energy Storage*, vol. 21, pp. 801-825, 2019.
4. BP p.l.c, "Statistical Review of World Energy," bp Statistical Review, 26 June 2023. [Online]. Available: https://www.bp.com/en/global/corporate/energy-economics/energy-outlook/renewable-energy.html.
5. B. Conway, *Electrochemical Supercapacitors - Scientific Fundamentals and Technological Applications*, 1st ed., Ottawa: Springer Science+Business Media, LLC, 1999, pp. 6-7.
6. A. González, E. Goikolea, J. Barrena and R. Mysyk, "Review on supercapacitors: Technologies and materials," *Renewable and Sustainable Energy Reviews*, vol. 58, pp. 1189-1206, May 2016.
7. J. Xie, P. Yang, Y. Wang, T. Qi, Y. Lei, and Chang Ming Li, "Puzzles and confusions in supercapacitor and battery: Theory and solutions," *Journal of Power Sources*, vol. 401, pp. 213–223, Oct. 2018.
8. J. R. Miller and P. Simon, "MATERIALS SCIENCE: Electrochemical Capacitors for Energy Management," *Science*, vol. 321, no. 5889, pp. 651–652, Aug. 2008.
9. P. Simon, Y. Gogotsi, and B. Dunn, "Where Do Batteries End and Supercapacitors Begin?," *Science*, vol. 343, no. 6176, pp. 1210–1211, Mar. 2014.
10. Luo, J. Y., Cui, W. J., He, P., & Xia, Y. Y. (2010). Raising the cycling stability of aqueous lithium-ion batteries by eliminating oxygen in the electrolyte. *Nature chemistry*, *2*(9), 760-765.
11. P. Sharma and T. Bhatti, "A review on electrochemical double-layer capacitors," *Energy Conversion and Management*, vol. 51, pp. 2901-2912, July 2010.
12. C. Costentin, T. Porter and J. Savéant, "How Do Pseudocapacitors Store Energy? Theoretical Analysis and Experimental Illustration," *ACS Applied Materials and Interfaces*, vol. 9, no. 10, pp. 8649-8658, 14 February 2017.
13. Y. Jiang and J. Liu, "Definitions of Pseudocapacitive Materials: A Brief Review," *Energy&Environmental Materials*, vol. 2, no. 1, pp. 30-37, March 2019.
14. D. P. Chatterjee and A. K. Nandi, "A review on the recent advances in hybrid supercapacitors," *Journal of Materials Chemistry A*, vol. 9, no. 29, pp. 15880–15918, 2021.
15. A. Nayak, B. Bhushan, S. Kotnala, N. Kukretee, P. Chaudhary, A. Tripathy, K. Ghai and S. Mudliar, "Nanomaterials for supercapacitors as energy storage application: Focus on its characteristics and limitations," *Materials Today: Proceedings*, vol. 73, no. 1, pp. 227-232, 2023.
16. Z. Yu, L. Tetard, L. Zhaia and J. Thomas, "Supercapacitor electrode materials: nanostructures from 0 to 3 dimensions," *Energy & Environmental Science*, vol. 8, pp. 702-730, 2015.
17. A. Muzaffar, M. B. Ahamed, K. Deshmukh and J. Thirumalai, "A review on recent advances in hybrid supercapacitors: Design, fabrication and applications," *Renewable and Sustainable Energy Reviews*, vol. 101, pp. 123-145, March 2019.
18. S. Venkateshalu, P. Goban Kumar, P. Kollu, S. K. Jeong, and A. N. Grace, "Solvothermal synthesis and electrochemical properties of phase pure pyrite FeS_2 for supercapacitor applications," *Electrochimica Acta*, vol. 290, pp. 378–389, Nov. 2018.
19. L. Pei, Y. Yang, H. Chu, J. Shen and M. Ye, "Self-assembled flower-like FeS_2/graphene aerogel composite with enhanced electrochemical properties," *Ceramics International*, vol. 42, no. 4, pp. 5053-5061, 2016.
20. I. K. Durga, S. S. Rao, R. M. Kalla, J.-W. Ahn and H.-J. Kim, "Facile synthesis of FeS_2/PVP composite as high-performance electrodes for supercapacitors," *Journal of Energy Storage*, vol. 28, pp. 101216, April 2020.
21. J. Chen, X. Zhou, C. Mei, J. Xu, S. Zhou and C. Wong, "Pyrite FeS_2 nanobelts as high-performance anode material for aqueous pseudocapacitor," *Electrochimica Acta*, vol. 222, pp. 172-176, 2016.
22. S. Zallouz, B. Réty, J.-M. L. Meins, M. Ndiaye, P. Fioux and C. Ghimbeu, "FeS_2 Nanoparticles in S-Doped Carbon: Ageing Effects on Performance as a Supercapacitor Electrode," *C — Journal of Carbon Research*, vol. 9, no. 4, pp. 112, 2023.
23. X. Liu, W. Deng, L. Liu, Y. Wang, C. Huang and Z. Wang, "Passion fruit-like microspheres of FeS_2 wrapped with carbon as an excellent fast charging material for supercapacitors," *New Journal of Chemistry*, vol. 46, pp. 11212-11219, 2022.
24. B. Li, L. Huang, M. Zhong, Z. Wei and J. Li, "Electrical and magnetic properties of FeS_2 and $CuFeS_2$ nanoplates," *RSC Advances*, vol. 5, no. 111, pp. 91103-91107, 2015.
25. W. Ding, X. Wang, H. Peng, Z. Peng and B. Dong, "Effect of Cu-doping on the electrochemical performance of FeS_2," *Materials Research Bulletin*, vol. 48, no. 11, pp. 4704-4710, 2013.
26. D. Pham, J. Baboo, J. Song, S. Kim, J. Jo, V. Mathew, M. H. Alfaruqi, B. Sambandama and J. Kim, "Facile synthesis of pyrite (FeS_2/C) nanoparticles as an electrode material for non-aqueous hybrid electrochemical capacitors," *Nanoscale*, vol. 10, no. 13, pp. 5938-5949, 2018.
27. Y. Wang, X. Zhang, Y. Ji, G. Zheng, J. Wang and F. Long, "Synthesis of M(M=Co^{2+}, Co^{2+}/Ni^{2+})-doped FeS_2 Nanospheres with Enhanced Visible-light-induced Photocatalytic Activity," *Journal of Wuhan University of Technology - Mater. Sci. Ed.*, vol. 33, p. 802–811, 2018.
28. G. Tang, J. Liang, and W. Wu, "Transition Metal Selenides for Supercapacitors," *Advanced Functional Materials*, Nov. 2023.
29. C. Debbarma, S. Radhakrishnan, S. M. Jeong, and C. S. Rout, "A comprehensive review on advanced supercapacitors based on transition metal tellurides: from material engineering to device fabrication," *Journal of Materials Chemistry A*, Jun. 2024.
30. J. Lu, F. Lian, L. Guan, Y. Zhanga and F. Ding, "Adapting FeS_2 micron particles as an electrode material for lithium-ion batteries via simultaneous construction of CNT internal networks and external cages," *Journal of Materials Chemistry A*, vol. 7, pp. 991-997, 2019.
31. M. Irham, O. Abdillah, D. Rodiansyah, F. Baskoro, H. Fahmi, T. Ogi and F. Iskandar, "Novel strategy for high-performance supercapacitors through the polyvinylpyrrolidone (PVP)-assisted in situ growth of FeS_2," *Dalton Transactions*, vol. 52, no. 25, pp. 8685-8694, 2023.
32. Y. Huang, S. Bao, Y. Yin and J. Lu, "Three-dimensional porous carbon decorated with FeS_2 nanospheres as electrode material for electrochemical energy storage," *Applied Surface Science*, vol. 565, p. 150538, November 2021.

33. S. Kokilavani, A. Syed, L. Raju, S. Al-Rashed, A. Elgorban, A. Thomas and S. S. Khan, "Synthesis of novel heterostructured FeS_2/Ag_2MoO_4 nanocomposite: Characterization, efficient antibacterial and enhanced visible light driven photocatalytic activity," *Surfaces and Interfaces*, vol. 23, p. 101003, April 2021.

34. T.-L. Yang, J.-Y. Chen, S.-W. Kuo, C.-T. Lo, and A. F. M. El-Mahdy, "Hydroxyl-Functionalized Covalent Organic Frameworks as High-Performance Supercapacitors," *Polymers*, vol. 14, no. 16, p. 3428, Aug. 2022.

35. Farkhod Azimov, J. Lee, S. Park, and Hyun Min Jung, "Fabrication of Assembled FeS_2 Nanosheet and Application for High-Performance Supercapacitor Electrodes," *ACS Applied Materials & Interfaces*, vol. 15, no. 22, pp. 26967–26976, May 2023.

36. X. Liu, L. Liu, W. Yan, Y. Wang, C. Huang, and Z. Wang, "Hierarchical Fe_3O_4@FeS_2 Nanocomposite as High-Specific-Capacitance Electrode Material for Supercapacitors," *Energy technology*, vol. 8, no. 10, Aug. 2020.

37. S. Hassanpoor and E. Tamri, "FeS_2/SRGO nanocomposite: Synthesis, characterization and comprehensive study of supercapacitor behavior in different electrolytes," *Journal of Alloys and Compounds*, vol. 932, p. 167711, Jan. 2023.

38. Syed Awais Ahmad *et al.*, "Facile synthesis of hierarchical ZnS@FeSe2 nanostructures as new energy-efficient cathode material for advanced asymmetric supercapacitors," *Journal of science. Advanced materials and devices/Journal of science. Advanced materials and devices (Print)*, vol. 7, no. 4, pp. 100489–100489, Dec. 2022.

39. Savithri Vishwanathan and S. Ramakrishna, "Low temperature synthesis of crystalline pyrite FeS_2 for high energy density supercapacitors," *Chemical communications*, vol. 59, no. 60, pp. 9263–9266, Jan. 2023.

40. M. Shirvani and Saied, "Bimetallic $CoSe_2/FeSe_2$ hollow nanocuboids assembled by nanoparticles as a positive electrode material for a high-performance hybrid supercapacitor," *Dalton Transactions*, vol. 51, no. 35, pp. 13405–13418, Jan. 2022.

41. N. Dey, D. Das, Samit Kumar Ray, and Prasanta Kumar Guha, "Analysis of the potential of nickel selenide micro-supercapacitors as energy storage device," *Journal of energy storage*, vol. 76, pp. 109722–109722, Jan. 2024.

42. S. S. Singha *et al.*, "Mn incorporated MoS_2 nanoflowers: A high performance electrode material for symmetric supercapacitor," *Electrochimica Acta*, vol. 338, p. 135815, Apr. 2020.

43. D. Zhang, Y. J. Mai, J. Y. Xiang, X. H. Xia, Y. Q. Qiao, and J. P. Tu, "FeS_2/C composite as an anode for lithium ion batteries with enhanced reversible capacity," *Journal of Power Sources*, vol. 217, pp. 229–235, Nov. 2012.

44. K. Kristmann *et al.*, "Characterization of FeS_2 pyrite microcrystals synthesized in different flux media," *Materials Advances*, vol. 5, no. 4, pp. 1565–1575, 2024.

45. M. Lu, *Supercapacitors: Materials, Systems, and Applications*. Weinheim: Wiley, 2013, pp. 111-120.

46. Y. Zeng, M. Yu, Y. Meng, P. Fang, X. Lu, and Y. Tong, "Iron-Based Supercapacitor Electrodes: Advances and Challenges," *Advanced Energy Materials*, vol. 6, no. 24, p. 1601053, Aug. 2016.

47. X. Li, L. Wu, L. Hao, and Y. Fu, "Emerging 2D Nanomaterials for Supercapacitor Applications," *Elsevier eBooks*, pp. 155–183, Jan. 2018.

48. G. F. Harrington and J. Santiso, "Back-to-Basics tutorial: X-ray diffraction of thin films," *Journal of Electroceramics*, Oct. 2021.

49. A. Dutta, "Fourier Transform Infrared Spectroscopy," *Spectroscopic Methods for Nanomaterials Characterization*, pp. 73–93, 2017.

50. G. C. King, *Physics of Energy Sources*. John Wiley & Sons, 2017.

51. S. Liu, M. Li, S. Li, H. Li, and L. Yan, "Synthesis and adsorption/photocatalysis performance of pyrite FeS_2," *Applied Surface Science*, vol. 268, pp. 213–217, Mar. 2013.

52. Jordi Jacas Biendicho *et al.*, "FeS_2-Decorated Carbon NanoFiber as Solid Phase Conversion-Type Cathode for Li-S Batteries," *Energies*, vol. 16, no. 11, pp. 4496–4496, Jun. 2023.